Acta Crystallographica Section B
Structural Science, Crystal Engineering and Materials
ISSN 2052-5206

High-pressure study of binary thorium compounds from first principles theory and comparisons with experiment

V. Kanchana,[a] G. Vaitheeswaran,[b] A. Svane,[c] S. Heathman,[d] L. Gerward[e]* and J. Staun Olsen[f]

[a]Department of Physics, Indian Institute of Technology Hyderabad, Ordnance Factory Estate, Yeddumailaram 502 205, Andhra Pradesh, India, [b]Advanced Centre of Research in High Energy Materials (ACRHEM), University of Hyderabad, Prof. C. R. Rao Road, Gachibowli, Andhra Pradesh, Hyderabad 500 046, India, [c]Department of Physics and Astronomy, Aarhus University, DK-8000 Aarhus-C, Denmark, [d]Eur-European Commission, Joint Research Centre, Institute for Transuranium Elements, Postfach 2340, D-76125 Karlsruhe, Germany, [e]Department of Physics, Technical University of Denmark, DK-2800 Lyngby, Denmark, and [f]Niels Bohr Institute, Ørsted Laboratory, DK-2100 Copenhagen, Denmark

Correspondence e-mail: gerward@fysik.dtu.dk

Received 12 September 2013
Accepted 5 May 2014

The high-pressure structural behaviour of a series of binary thorium compounds ThX (X = C, N, P, As, Sb, Bi, S, Se, Te) is studied using the all-electron full potential linear muffin-tin orbital (FP-LMTO) method within the generalized gradient approximation (GGA) for the exchange and correlation potential. The calculated equlibrium lattice parameters and bulk moduli, as well as the equations of state agree well with experimental results. New experiments are reported for ThBi and ThN. Calculations are performed for the ThX compounds in the NaCl- and CsCl-type crystal structures, and structural phase transitions from NaCl to CsCl are found in ThP, ThAs, ThSb and ThSe at pressures of 26.1, 22.1, 8.1 and 23.2 GPa, respectively, in excellent agreement with experimental results. ThC, ThN and ThS are found to be stable in the NaCl structure, and ThBi and ThTe in the CsCl structure, for pressures below 50 GPa. The electronic structures of the ThX compounds are studied using the quasiparticle self-consistent GW method (G: Green function, W: dynamically screened interaction).

1. Introduction

Compounds of thorium with non-metals are promising nuclear materials for reactor composites and high-strength structures. An important class of material is represented by the ceramics based on the binary thorium compounds ThX with 2p–4p elements (X = C, N, P, As, Sb, Bi, O, S, Se, Te). At ambient conditions they have the NaCl ($B1$) crystal structure, with the exceptions of ThBi and ThTe, which are found in the CsCl ($B2$) crystal structure (Borzone *et al.*, 1982). The structural properties under high pressure have been the subject of a number of investigations (Benedict *et al.*, 1984; Gerward *et al.*, 1985, 1986, 1988; Gerward, Olsen, Steenstrup *et al.*, 1990; Olsen *et al.*, 1988, 1989; Gerward, Olsen, Benedict & Luo, 1990). Structural transitions from the $B1$ structure to the $B2$ structure are observed in ThP at a pressure of 20 GPa (Olsen *et al.*, 1989), in ThAs at a pressure of 18 GPa (Gerward *et al.*, 1988), in ThSb at a pressure of 9 GPa (Gerward *et al.*, 1988), and in ThSe at a pressure of 15 GPa (Olsen *et al.*, 1988). In ThS a second-order structural transition to a distorted NaCl structure is seen above a pressure of 20 GPa (Benedict *et al.*, 1984). For ThC (Gerward *et al.*, 1986; Gerward, Olsen, Benedict & Luo, 1990) and ThN (Gerward *et al.*, 1985) the $B1$ structure is found to be stable in the pressure range 0–50 GPa. The systematics of these results are discussed by several authors (Borzone *et al.*, 1982; Olsen *et al.*, 1986; Benedict *et al.*, 1989; Gerward, Olsen, Steenstrup *et al.*, 1990; Gensini, 1994). A detailed review of the comparitive aspects of the high-pressure behaviour of lanthanide and actinide compounds was given by Benedict (1995). Optical phonon frequencies of ThX

compounds have been measured by Wedgwood (1974) using neutron scattering.

From the theoretical side, trends in the electronic structure of the actinide mononitrides were studied, using the linear muffin-tin orbital (LMTO) method (Brooks, 1984; Petit *et al.*, 2009) or the full-potential linear augmented plane wave (LAPW) method (Atta-Fynn & Ray, 2007) with emphasis on the role of the 5*f* electrons and their localized/delocalized character. The Fermi surface of ThC was calculated with the self-consistent relativistic augmented plane wave method by Hasegawa & Yamagami (1990) who found ThC to be a semimetal. The optical conductivity spectrum and dielectric response of thorium monopnictides were calculated with the LMTO method (Kumar & Auluck, 2003). The elastic properties of thorium monopnictides, monochalcogenides and tetrapnictides were studied with the LAPW method by Shein *et al.* (2007) and Shein & Ivanovskii (2010). Recently, first-principles calculations of vibrational and structural properties of ThN up to 100 GPa were studied, and a phonon softening under pressure was predicted to occur (Modak & Verma, 2011). Apart from these density-functional-based calculations, the interionic potentials approach has been used to study the high-pressure behaviour of binary thorium pnictides and chalcogenides (Aynyas, Sanyal & Jha, 2002; Aynyas, Kaurav & Sanyal, 2002; Gupta & Singh, 2010).

In the present work the high-pressure structural phase transitions of Th*X* (*X* = C, N, P, As, Sb, Bi, S, Se, Te) compounds are investigated by *ab intio* calculations using the LMTO method with the generalized gradient approximation to treat exchange and correlation effects. The structural phase stability of the Th*X* compounds is analyzed and the transition pressures from *B*1 to *B*2 structures are obtained. We compare with reported as well as new experimental results. The pressure–volume relation is calculated and the volume collapse associated with the structural phase transition is extracted. The paper is organized in the following way: the computational method is described in §2, results are presented and discussed in §3, and §4 concludes the paper.

2. Methodologies

2.1. Computational details

In this work the LMTO method (Andersen, 1975) in the all-electron full-potential (FP-LMTO) implementation of Savrasov (1996) is employed to calculate the total energies and basic ground-state properties of the thorium monopnictides and monochalcogenides. In this method the crystal is divided into two regions: non-overlapping muffin-tin spheres surrounding each atom and the interstitial region between the spheres. We used a double κ *spdf* LMTO basis (each radial function within the muffin-tin spheres is matched to a Hankel function in the interstitial region with decay constant κ). The calculations included the (7*s*, 6*s*, 6*p*, 6*d*, 5*f*) partial waves for Th, (2*s*, 2*p*) partial waves for C and N, (3*s*, 3*p*, 3*d*) partial waves for P and S, (4*s*, 4*p*, 3*d*, 4*d*) partial waves for As and Se, (5*s*, 5*p*, 4*d*, 5*d*) partial waves for Sb and Te, and (6*s*, 6*p*, 5*d*) partial waves for Bi, respectively. The exchange–correlation potential was calculated within the generalized gradient approximation (GGA; Perdew *et al.*, 1996). The charge density and the potential inside the muffin-tin spheres were expanded in terms of spherical harmonics up to $\ell_{\max} = 6$, while in the interstitial region they were expanded in terms of plane waves. A total of 6566 plane waves (energy up to 131.42 Ry) were included in the NaCl structure and 7152 plane waves (energy up to 104.18 Ry) in the CsCl structure. Total energies were calculated as a function of volume for a (24,24,24) *k* mesh containing 413 (455) *k*-points in the irreducible wedge of the Brillouin zone for the NaCl (CsCl) structure. The total energies are fitted to the Birch equation-of-state (Birch, 1947) to obtain the theoretical equilibrium volume, bulk modulus and the transition pressure. The calculations were scalar-relativistic, implying that all relativistic effects except spin-orbit coupling have been included in the evaluation of the total energy. The spin-orbit coupling is a significant energy for the one-electron energies in actinides, however, the spin-orbit coupling does not vary much with volume, so it will have little effect on the ground-state properties, which are studied in the present work. The band structures and Fermi surfaces were calculated *with* the spin-orbit coupling included. A critical discussion of schemes of implementation of spin-orbit coupling in muffin-tin-based electronic structure calculations was given by Nordström *et al.* (2000), see also Kanchana *et al.* (2006). Atta-Fynn & Ray (2007) investigated the equilibrium lattice constants and bulk moduli of actinide nitrides using the GGA with and without spin-orbit coupling included. For ThN they only found minor changes in these properties, while the effects were larger in the later actinide nitrides.

The electronic structure including spin-orbit coupling is calculated using the quasiparticle self-consistent *GW* approximation (QSGW; *G*: Green's function, *W*: screened interaction; Kotani *et al.*, 2007). The *GW* approximation (Hedin & Lundqvist, 1969) is formally the first term in an expansion of the non-local and energy-dependent self-energy $\Sigma(\mathbf{r}, \mathbf{r}', \omega)$ in the screened Coulomb interaction *W*. A more physically appealing picture views the *GW* as a dynamically screened Hartree–Fock approximation plus a Coulomb hole contribution (Hedin & Lundqvist, 1969).

The QSGW was implemented in the FP-LMTO method of Methfessel *et al.* (2000), which also includes a double κ LMTO basis set. For an accurate description of the polarization function the basis set has been augmented with high-lying ligand *s* and *p* states as well as interstitial 'floating' orbitals (Methfessel *et al.*, 2000). Furthermore, inside muffin-tin spheres a product basis set has been used (Aryasetiawan & Gunnarsson, 1994). An $8 \times 8 \times 8$ Monkhorst–Pack (MP) *k*-mesh is used for the calculation of the screened interaction, which is evaluated in the random phase approximation. The special feature of the quasiparticle selfconsistency is that the one-particle band structure, which is used as input to the evaluation of the *GW* eigenenergies, is iterated so as to come as close as possible to the output band *GW* structure (Kotani *et al.*, 2007).

2.2. Experimental

High-pressure structural investigations were conducted on two imperfect samples, one containing the binary ThN and the other containing ThBi. Both experiments were performed at the EDS F3 beamline of HASYLAB (DESY synchrotron, Hamburg, Germany) with an energy dispersive Ge detector system. The measurements were made at room temperature on powdered samples using a Syassen–Holzapfel-type diamond–anvil cell. Microsamples of the materials were loaded into 0.2 mm holes drilled into an annealed and pre-indented Inconel gasket along with a ruby splinter for pressure determination. Silicone oil was used as the pressure transmitting medium.

The prepared ThBi sample showed a mixture of phases. We were able to determine the presence at ambient pressure of cubic CsCl-type ThBi (with lattice parameter a = 3.9635 Å), although this was only about 20% of the bulk. The rest comprised unreacted Th metal and one other minor phase which could not be characterized as either of the known $ThBi_2$ or Th_3Bi_4 structures. We were able to follow the CsCl phase under pressure up to 18 GPa and could obtain approximate Birch and Murnaghan compressibilities for this phase. The presence of so much unreacted Th metal in the sample may affect the compressibility of the remaining ThBi although the pure Th metal is relatively soft with a bulk modulus of between 60 and 63 GPa compared with the measured bulk modulus of 211–212 GPa for the ThBi fraction of the bulk sample.

Studies were also carried out on ThN where, as in the case of ThBi, the sample actually comprised a mixture of ThN and Th plus a small quantity of Ta from the sample preparation crucible. In this case the ThN fraction comprised ~ 60% of the bulk material and due to the differing compressibilities of ThN and Th we were able to follow the behaviour of both constituents up to 20 GPa until the diffraction peaks overlapped.

The results of the present experiments are included in Table 1.

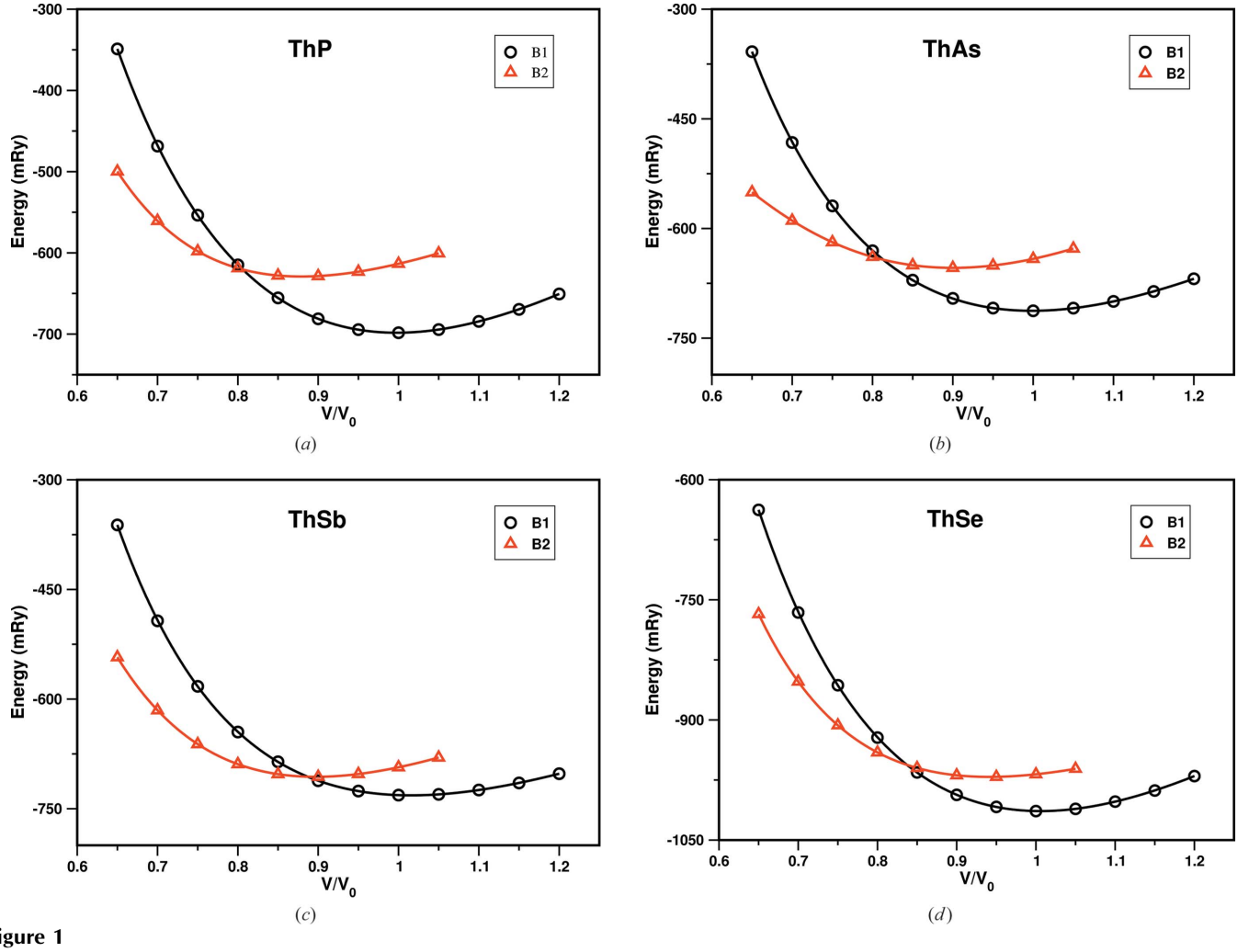

Figure 1
Variation of the total energy with the volume for the $B1$ and $B2$ structures of (*a*) ThP, (*b*) ThAs, (*c*) ThSb and (*d*) ThSe. Volumes are given relative to the experimental equilibrium volumes, as given by the experimental lattice constants quoted in Table 1. Energies are quoted in units of mRy per formula unit.

Table 1
Calculated lattice constants (in Å) and bulk moduli (in GPa) of ThX (X = C, N, P, As, Sb, Bi, S, Se, Te) compounds.

Experimental results obtained in the present work as well as reported in the past are included for comparison.

		Lattice constant (Å)		Bulk modulus (GPa)	
Compound	Structure	Theory	Expt.	Theory	Expt
ThC	*B*1	5.310	5.322[a]	148.9	109[a]
ThN	*B*1	5.156	5.160[b], 5.167[c]	201.7	211[b], 175[c]
ThP	*B*1	5.822	5.827[d]	136.0	137[d]
ThAs	*B*1	5.975	5.978[e]	119.0	118[e]
ThSb	*B*1	6.351	6.318[e]	83.7	84d
ThBi	*B*2	3.922	3.964[b], 3.909[f]	81.2	173[b]
ThS	*B*1	5.704	5.685[g]	172.6	145[g]
ThSe	*B*1	5.901	5.890[h]	131.5	125[h]
ThTe	*B*2	3.838	3.827[h]	92.2	102[h]

References: (*a*) Gerward *et al.* (1986); (*b*) this work; (*c*) Gerward *et al.* (1985); (*d*) Olsen *et al.* (1989); (*e*) Gerward *et al.* (1988); (*f*) Borzone *et al.* (1982); (*g*) Benedict *et al.* (1984); (*h*) Olsen *et al.* (1988).

3. Results and discussion

3.1. Ground-state properties

The total energies as a function of relative volume are calculated for all the thorium pnictides and chalcogenides in the *B*1 and *B*2 phases and examples are plotted in Fig. 1. The calculated total energies are fitted to the Birch equation-of-state to obtain the basic ground-state properties. The calculated lattice constants and the bulk moduli of the ThX compounds in the NaCl structure are reported in Table 1 along with the experimental values. As stated earlier, ThTe and ThBi crystallize in the *B*2-type structure and their ground-state properties are also reported in Table 1. As evident from the table, the calculated lattice constants are found to be in excellent agreement with the experimental values and the deviations obtained in the calculated bulk moduli are well within the usual error bars of the GGA.

The present experimental value for the bulk modulus of ThN, B = 211 GPa, agrees well with the theoretical value, B = 201.7 GPa. It is also seen that this value and an earlier experimental result enclose the theoretical prediction. Previous theoretical works calculated the bulk modulus of ThN to be B = 178 GPa (Atta-Fynn & Ray, 2007) and B = 180.8 GPa (Modak & Verma, 2011), in both cases using the same GGA functional as used here, however, implemented in different electronic structure schemes.

3.2. Structural phase transitions

From the total energy curves plotted in the *B*1- and *B*2-type structures for all the ThX compounds, it is evident that all the compounds have NaCl-type structures under ambient conditions, except ThBi and ThTe which are found to crystallize in the *B*2-type structure. A first-order structural phase transition from *B*1- to *B*2-type structures is found to occur around 26.1, 22.1, 8.1 GPa for ThP, ThAs and ThSb, respectively. The calculated pressure–volume relations are shown in Figs. 2 and 3, and compared with experimental data (Gerward *et al.*, 1985, 1988; Gerward, Olsen, Benedict & Luo, 1990; Olsen *et al.*, 1988, 1989). Generally, agreement between theory and experiment is fine, however, in the details there are several discrepancies. For ThC, Fig. 2(*a*), the calculated compression curve indicates a significantly harder behaviour than the observed one. For ThN, Fig. 2(*b*), the agreement between

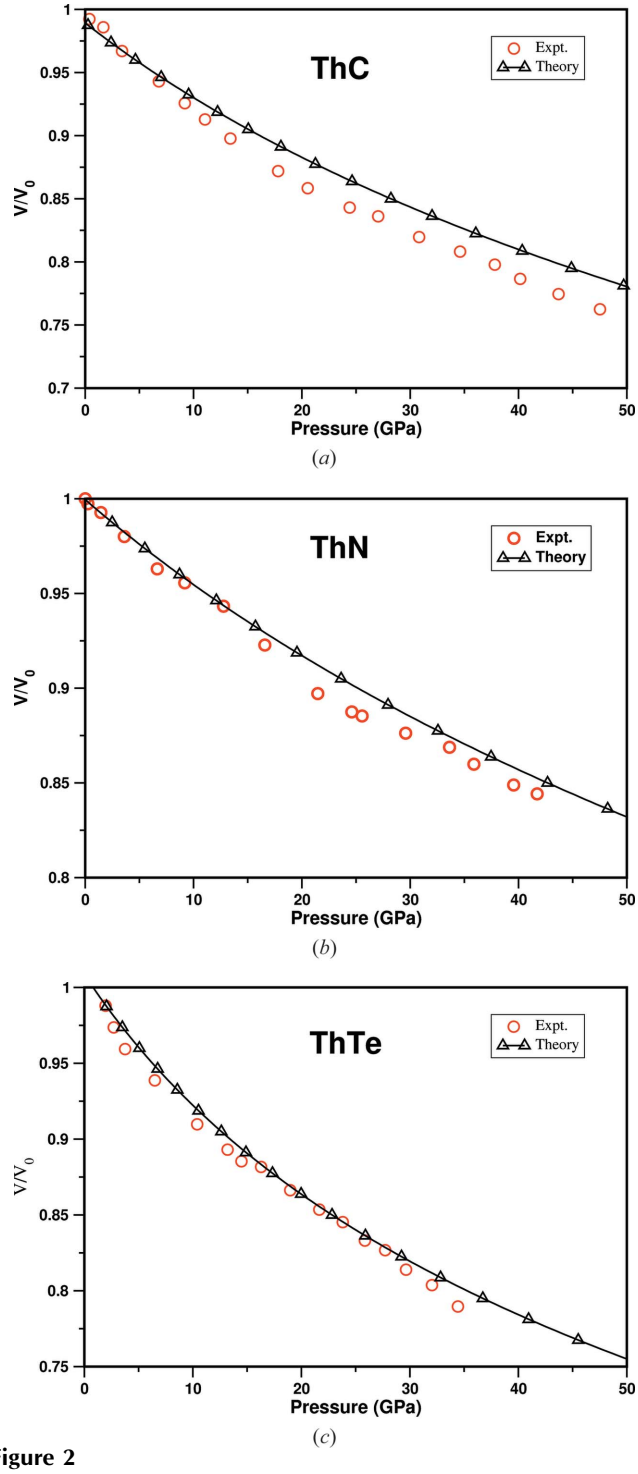

Figure 2
Variation of relative volume with pressure for (*a*) ThC, (*b*) ThN and (*c*) ThTe. Volumes are given relative to the experimental equilibrium volumes, as given by the experimental lattice constants quoted in Table 1. Experimental data are from: ThC: Gerward, Olsen, Benedict & Luo (1990); ThN: Gerward *et al.* (1985); ThTe: Olsen *et al.* (1988).

theory and experiment is excellent from 0–15 GPa, from which again the calculated curve indicates a slightly harder behaviour than the measured curve. In ThTe, Fig. 2(*c*), theory and experiment agree well in the entire range to 35 GPa covered by experiment. ThP, ThAs, ThSb and ThSe all exhibit the *B*1 → *B*2 structural transition at elevated pressures, in theory as well as in experiment, as illustrated in Fig. 3. The calculated transition pressure from *B*1 to *B*2 and the volume collapse associated with the transition are quoted in Table 2, which shows good agreement with the experimental data. The pressure–volume relation of ThSb, Fig. 3(*c*), at low pressures differs with respect to experiment mainly due to the slightly larger equilibrium lattice constant calculated for this compound.

At high pressures, the agreement between theory and experiment for the *B*2 phase of ThP, Fig. 3(*a*), and ThAs, Fig. 3(*b*), is less satisfactory. One notices a particularly hard *B*2 phase of ThP according to experiment, and significant scatter in the experimental data points for ThAs. Experimentally, ThC and ThN, which crystallize in the *B*1 structure, are found to remain stable in this structure up to 50 and 47 GPa (Gerward, Olsen, Benedict & Luo, 1990; Gerward *et al.*, 1985), respectively, in agreement with the present theory. Modak & Verma (2011) predicted a *B*1 → *B*2 structural transition to occur for ThN at a pressure of 72.5 GPa, which is larger than the pressure range within which ThN until now has been studied experimentally.

Among the thorium chalcogenides, ThS crystallizes in the *B*1 structure and was in the present theoretical investigation not found to undergo a structural phase transition to the *B*2 phase at high pressure. Experimentally, a distorted *B*1 phase

Table 2
Calculated and experimental transition pressure P_t (GPa) and volume changes given in % for the *B*1 to *B*2 structural phase transitions in Th*X* (*X* = P, As, Sb, Se).

	P_t		Volume collapse (%)	
Compound	Theory	Expt.	Theory	Expt
ThP	26.1	30[a]	13.3	11.9[a]
ThAs	22.1	18[b]	14.9	10[b]
ThSb	8.1	9–10[b]	11.1	9.4[b]
ThSe	23.2	15–20[c]	9.4	9.1[c]

References: (*a*) Olsen *et al.* (1989); (*b*) Gerward *et al.* (1988); (*c*) Olsen *et al.* (1988).

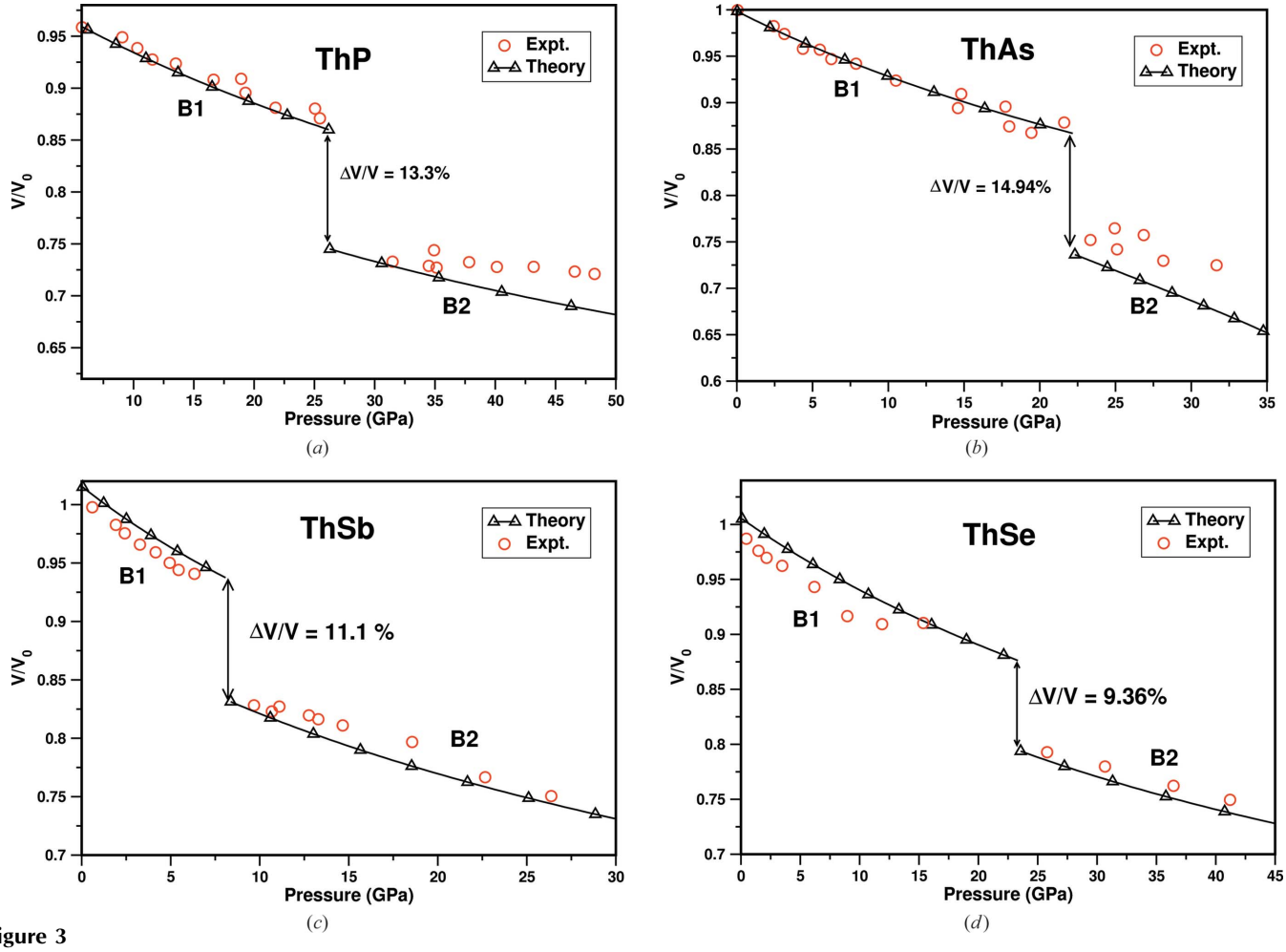

Figure 3
Variation of relative volume with pressure for (*a*) ThP, (*b*) ThAs, (*c*) ThSb and (*d*) ThSe. Volumes are given relative to the experimental equilibrium volumes, as given by the experimental lattice constants quoted in Table 1. Experimental data are from: ThP: Olsen *et al.* (1989); ThAs and ThSb: Gerward *et al.* (1988); ThSe: Gerward *et al.* (1988).

has been observed above 20 GPa (Benedict *et al.*, 1984). ThSe undergoes a *B*1 to *B*2 transition around 23.2 GPa with a volume collapse of 9.4%, as illustrated in Fig. 3(*d*). In contrast ThTe crystallizes in the *B*2 stucture already at ambient pressure. These findings reflect the general rule that the *B*2 phase becomes more favourable when the sizes of the atomic constituents become similar.

3.3. Band structure and Fermi surface

To elucidate the electronic structures of the Th*X* compounds this section shows examples of calculated band structures and Fermi surfaces. The calculations were all performed at the experimental lattice constants (Table 1). While the theoretical and experimental lattice constants differ slightly, the electronic structure does not change significantly on that scale. In fact, the electronic structure is rather robust

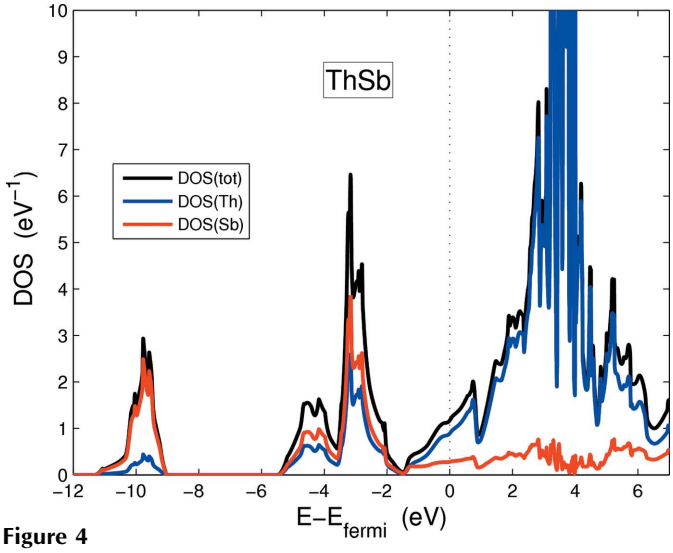

Figure 4
Density-of-states for ThSb at the ambient *B*1 lattice parameter and in units of states per unit cell and per eV. The QSGW approximation was used and spin-orbit coupling included. The zero of energy is placed at the Fermi level. The partial contributions of Th and Sb are shown in blue and red, respectively.

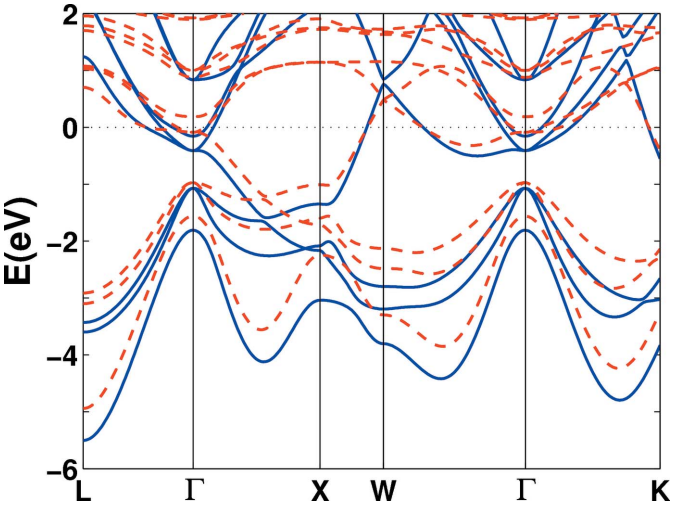

Figure 5
Band structure of ThSb in the ambient *B*1 crystal structure; blue line as calculated in the QSGW approxmation and red line as calculated with the LDA. The calculations include spin-orbit coupling. The zero of energy is placed at the Fermi level.

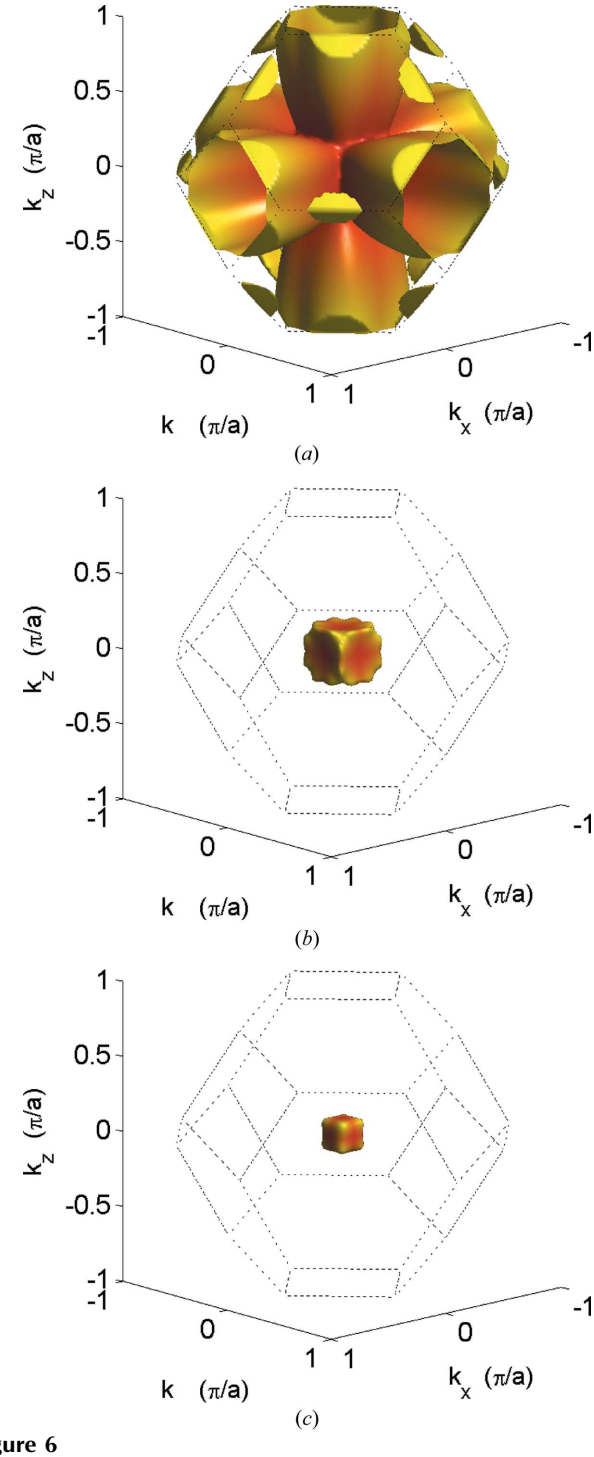

Figure 6
The calculated QSGW Fermi surface of ThSb, with spin-orbit coupling included. The first sheet (*a*) may be viewed as large electron ellipsoids centred at the *X*-points and merging together at the Γ-point. The second (*b*) and third (*c*) sheets are electron pockets around Γ. The first Brillouin zone is indicated by thin dotted lines. The colouring is only for presentation purposes.

towards compression implying that no significant charge transfer occurs under pressure, and the structural transformations discussed in §3.2 seem not to be associated with any peculiar Fermi surface behaviour, such as topology change.

The electronic structures of the thorium monopnictides are all very alike, and exemplified by ThSb in Figs. 4–6. The density of states, calculated with the QSGW method, in Fig. 4 shows the Sb *s*-bands around 10 eV below the Fermi level and the Sb *p*-dominated valence bands between −5.5 and −2 eV. The bands around the Fermi level are dominated by Th *d* states with some admixture of Th *f*. The Th *f* bands fall around 4 eV above the Fermi level. The band structure of ThSb is shown in Fig. 5, where the QSGW and LDA band structures are compared (only a narrow part around the Fermi level is shown). It is noticeable that the QSGW valence bands are wider, by ∼ 0.5 eV, than the LDA bands, and the unoccupied Th *f* states lie about 2 eV higher in QSGW than in LDA. In the vicinity of the Fermi level very little change occurs, except close to the Γ point.

Other noticible differences in the electronic structure of ThSb between QSGW and LDA are the large downwards shifts in QSGW of the Sb 5*s* band (by about 0.6 eV) as well as the Sb 4*d* [by about 3.5 eV, $\epsilon(4d_{3/2})$ = −32.7 eV, $\epsilon(4d_{5/2})$ = −31.3 eV (relative to the Fermi level)] and the Th 6*p* semi-core states [by ∼ 1.5 eV, $\epsilon(6p_{1/2})$ = −27.4 eV, $\epsilon(6p_{3/2})$ = −16.5 eV (relative to the Fermi level)]. For comparison, the experimental position of the thorium 6*p* levels are −25.8 and −17.3 eV in oxidized thorium films (Fuggle *et al.*, 1974), in reasonable agreement. Apparently the theoretical spin-orbit splitting is somewhat larger than that measured; one possible reason for this being the insufficient treatment of the shape of the relativistic $6p_{1/2}$ orbital (Nordström *et al.*, 2000). The Fermi surface of ThSb is illustrated in Fig. 6. There are three sheets, the first one being the large egg-shaped electron pockets around the *X*-points, which merge together close to Γ. The second and third sheets are small electron pockets around the

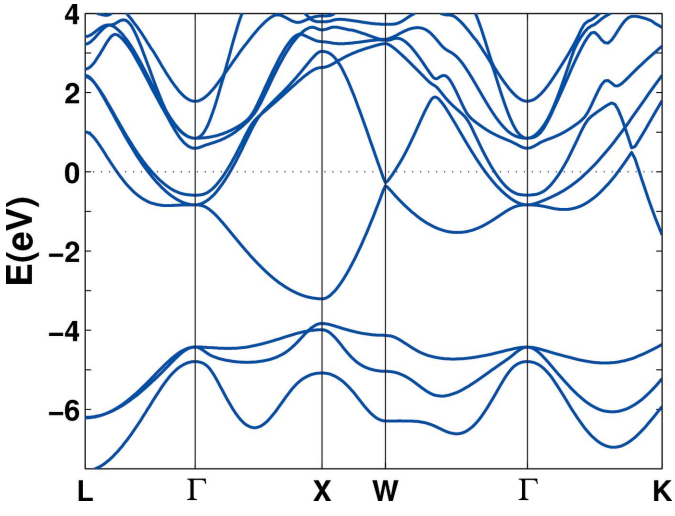

Figure 7
Band structure of ThS in the ambient *B*1 crystal structure, as calculated in the QSGW approxmation and with spin-orbit coupling included. The zero of energy is placed at the Fermi level.

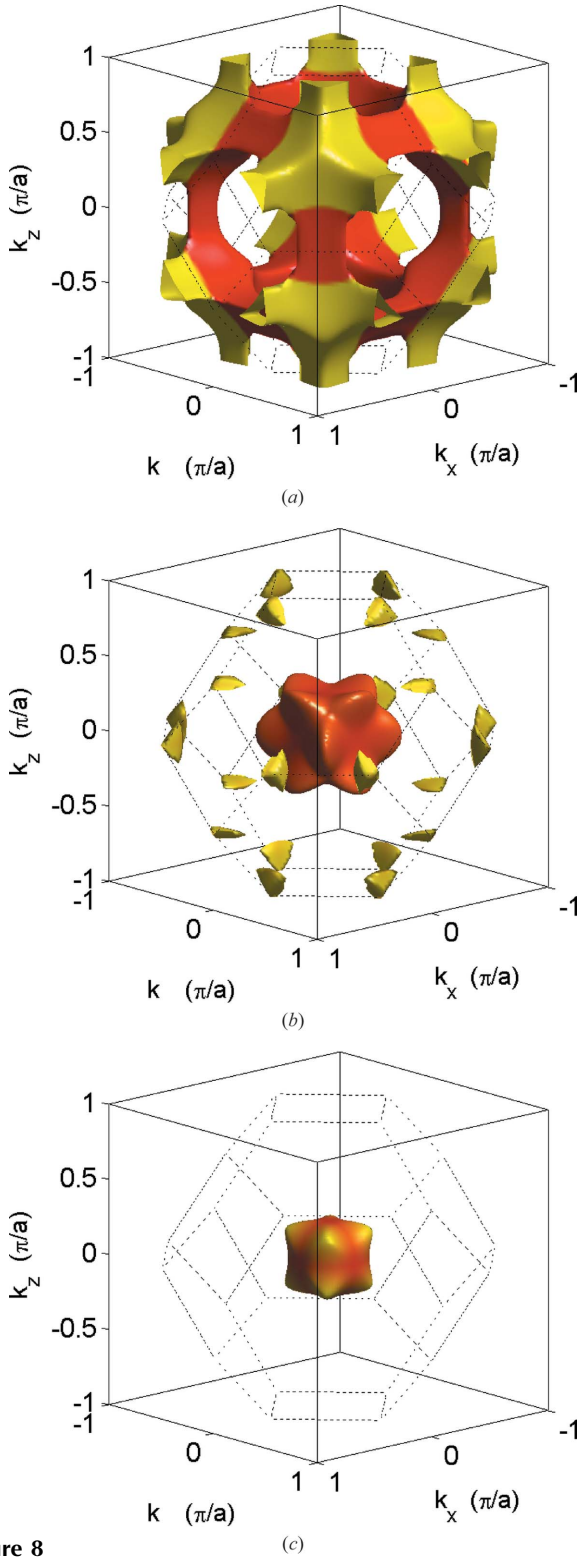

Figure 8
The calculated QSGW Fermi surface of ThS, with spin-orbit coupling included. The first sheet in (*a*) can be viewed as a quasi-cubic system of filaments of hole character with corners in the *L*-points ($\pi/a(1/2, 1/2, 1/2)$) of the Brillouin zone. The second (*b*) and third (*c*) sheets are electron pockets around Γ, in the case of (*b*) additional electron pockets around the *W*-points ($\pi/a(1, 1/2, 0)$) appear. The first Brillouin zone is indicated by thin dotted lines. In (*a*) the colouring is used to illustrate the part belonging to the first Brillouin zone (dark, reddish) and the part belonging to the exterior of the first Brillouin zone (light, yellowish). In (*b*) and (*c*) the colouring is only for presentation purposes.

Γ point, which are due to the bands dipping below the Fermi level close to Γ in Fig. 5. Note that at the Γ point, the electron eigenenergies are lower in QSGW than in LDA, so the third Fermi sheet would not exist according to LDA, and the second sheet would be smaller. Similarly, these states lie higher relative to the Fermi level in the earlier pnictides (as calculated in QSGW as well as in LDA). Hence the third sheet is very small in ThAs and absent in ThP and ThN; in the latter case even the second sheet is absent. The first sheet remains more or less of the same shape in all thorium monopnictides. A similar Fermi surface was found for CeN (Kanchana *et al.*, 2011). For ThN, these findings were also discussed by Modak & Verma (2011).

The band structure of ThS is shown in Fig. 7. The overall topology is similar to that of the ThSb bands in Fig. 5, apart from the position of the Fermi level, which is higher in ThS due to the higher number of valence electrons. In ThS a gap appears between the S *p* bands (situated between −7 and −4 eV) and the Th bands starting at −3.2 eV. The ThS Fermi surface is shown in Fig. 8. The first sheet is characterized by a quasicubic filamental structure of hole character, similar to what may be found in the iso-electronic and iso-structural Pb*X* compounds (Svane *et al.*, 2010). The second and third sheets are electron pockets around the Γ point with some additional small pockets around the W-point. These are equivalents of the smaller electron pockets in Figs. 6(*b*) and (*c*). The ThSe band structure and Fermi surface are very similar to ThS and is not shown.

The band structure of ThTe in the ambient *B*2 is shown in Fig. 9. The band structure is different from the ThSb and ThS cases in Figs. 5 and 7, due to the different crystal structure. The trends in differences between the LDA and GW band structures are the same though: in QSGW the Te *p*-band is widened by about 0.5 eV, and the centroid of the Th *f* states are shifted ∼ 2 eV further above the Fermi level. The bands crossing the Fermi level are very alike, hence the LDA and QSGW Fermi surfaces are very alike. The QSGW Fermi surface of ThTe is illustrated in Fig. 10, showing two sheets, hole pockets centred around the *R*-point and electron pockets around the Γ-point. The ThBi band structure is similar to ThTe, see Fig. 11(*a*). Due to the lower valence electron count, only one Fermi surface sheet is seen, Fig. 11(*b*), which is an enlarged counterpart of the first sheet of ThTe, Fig. 10(*a*). Additional small electron pockets appear around the Γ- and *M*-points.

ThC exhibits a semimetallic band structure as already discussed by Hasegawa & Yamagami (1990), with hole pockets around the *X*-point of the Brillouin zone and electron pockets in the interior of the Brillouin zone, centred on the Γ–*X* lines. The present GW calculations find the same electronic struc-

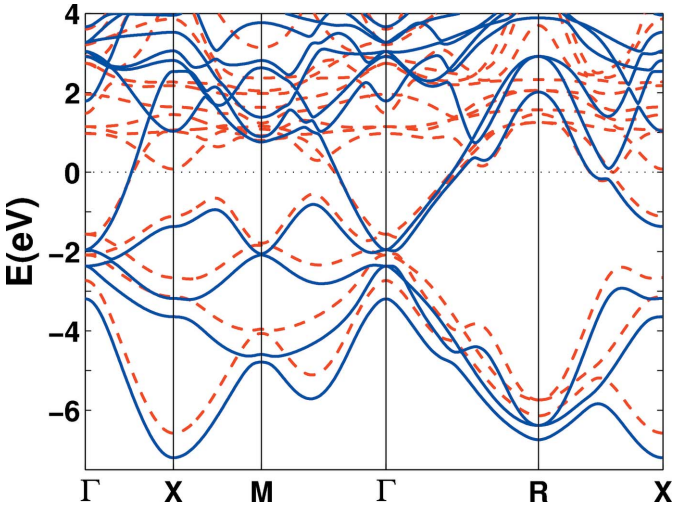

Figure 9
Band structure of ThTe in the ambient *B*2 crystal structure, as calculated in the QSGW approxmation with spin-orbit coupling included. The LDA bands are shown in dashed (red). The zero of energy is placed at the Fermi level.

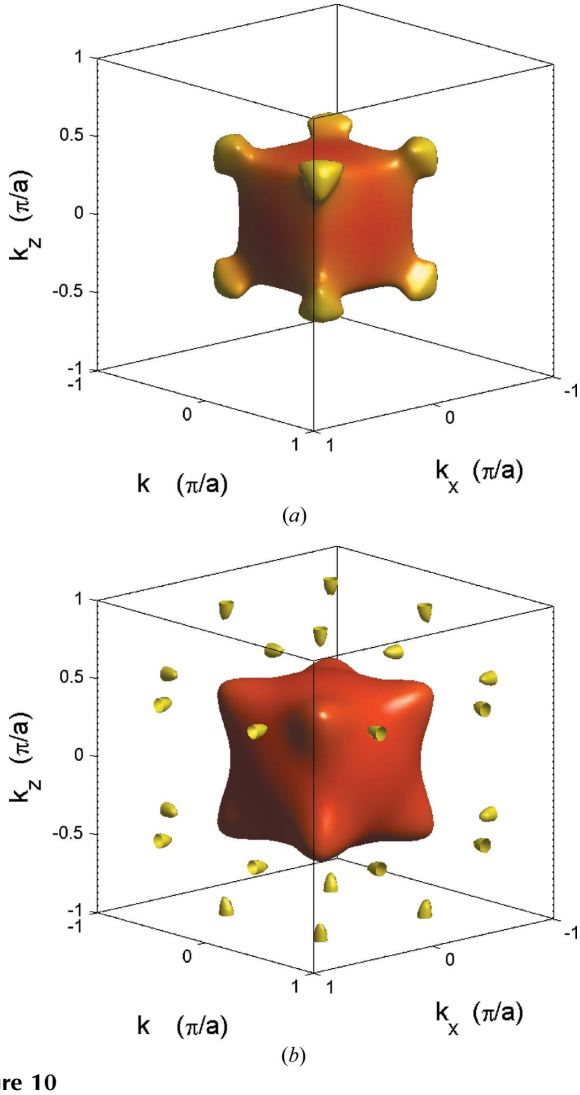

Figure 10
The calculated QSGW Fermi surface of ThTe in the *B*2 structure, with spin-orbit coupling included. In (*a*) the centre of the cubic Brillouin zone corresponds to the *R*-point $(\pi/a(1, 1, 1))$, *i.e.* the first sheet corresponds to hole pockets around the *R*-point. In (*b*) the centre corresponds to the Γ point, and the second sheet corresponds to a large electron pockets around Γ with some additional small pockets at the Brillouin zone faces. The colouring is only for presentation purposes.

ture (not shown). The electron and hole pockets are found to slightly increase in size under pressure.

4. Summary and conclusions

A theoretical investigation of the high-pressure behaviour and structural phase transitions in ThX compounds (X = N, P, As, Sb, Bi, S, Se and Te) has been presented and compared with new experimental results for ThN and ThBi as well as experimental results reported in the literature. The $B1 \rightarrow B2$ structural transition is found in ThP, ThAs, ThSb and ThSe at transition pressures of 26.1, 22.1, 8.1 and 23.2 GPa, respectively, in good agreement with the experimentally observed transitions in these compounds. ThBi and ThTe already crystallize in the $B2$ structure at ambient conditions, while no $B1 \rightarrow B2$ transition was observed for ThC, ThS and ThN up to 50 GPa. The electronic structure of the ThX compounds was discussed using the quasiparticle band structure as obtained with the QSGW method.

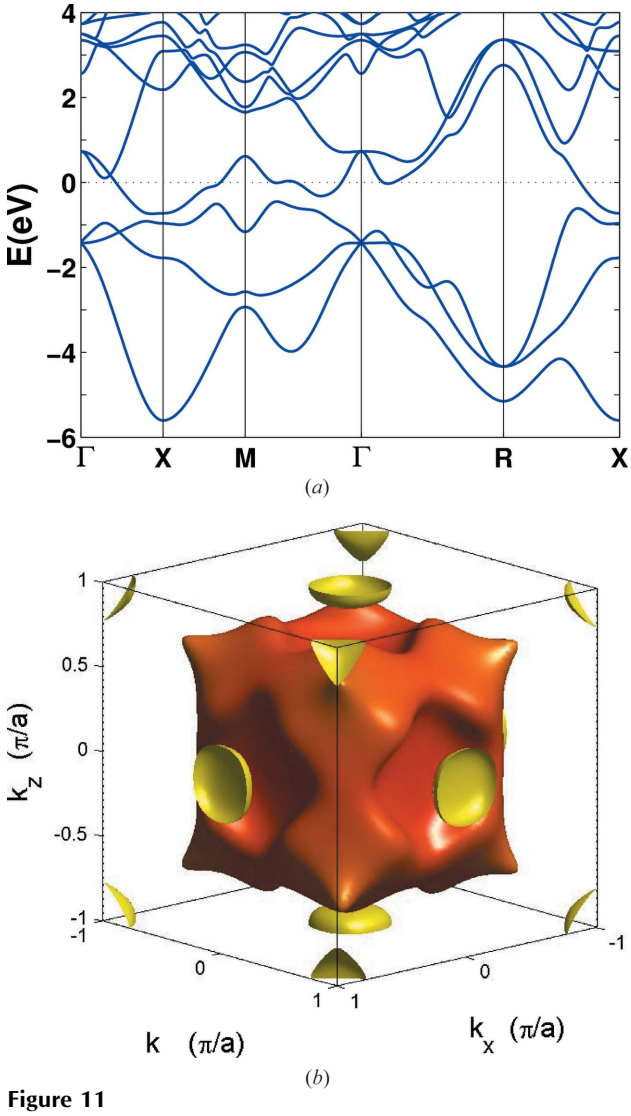

Figure 11
The calculated QSGW band structure (*a*) and Fermi surface (*b*) of ThBi in the $B2$ structure, with spin-orbit coupling included. In (*b*) the centre of the cubic Brillouin zone corresponds to the R-point ($\pi/a(1, 1, 1)$), *i.e.* the Fermi surface consists of large hole pockets around the R point, with smaller hole pockets around Γ and M ($\pi/a(1, 1, 0)$). The colouring is only for presentation purposes.

AS acknowledges support from the Danish Center for Scientific Computing Center and the Danish Agency for Science, Technology and Innovation. LG and JSO acknowledge support from the Danish Natural Science Research Council through DANSYNC and DANSCATT.

References

Andersen, O. K. (1975). *Phys. Rev. B*, **12**, 3060–3083.
Aryasetiawan, F. & Gunnarsson, O. (1994). *Phys. Rev. B*, **49**, 16214–16222.
Atta-Fynn, R. & Ray, A. K. (2007). *Phys. Rev. B*, **76**, 115101.
Aynyas, M., Sanyal, S. P. & Jha, P. K. (2002). *Phys. Status Solidi B*, **229**, 1459–1466.
Aynyas, M., Kaurav, N. & Sanyal, S. P. (2002). *J. Phys. Chem. Solids* **63**, 821–826.
Benedict, U., Spirlet, J. C., Gerward, L. & Olsen, J. S. (1984). *J. Less. Commun. Metals*, **98**, 301–307.
Benedict, U., Dabos-Seignon, S., Dufour, C., Luo, H. & Heathman, S. (1989). *J. Nucl. Mater.* **166**, 48–55.
Benedict, U. (1995). *J. Alloys Compds*, **223**, 216–225.
Birch, F. (1947). *Phys. Rev.* **54**, 809–824.
Borzone, G., Borsese, A. & Ferro, R. (1982). *J. Less-Common. Met.* **84**, 195–203.
Brooks, M. S. S. (1984). *J. Phys. Metal Phys.* **14**, 857–871.
Fuggle, J. C., Burr, A. F., Watson, L. M., Fabian, D. J. & Lang, W. (1974). *J. Phys. Metal Phys.* **4**, 335–342.
Gensini, M. (1994). *J. Alloys Compds*, **213/214**, 391–393.
Gerward, L., Staun Olsen, J., Benedict, U., Itié, J.-P. & Spirlet, J. C. (1985). *J. Appl. Cryst.* **18**, 339–341.
Gerward, L., Staun Olsen, J., Benedict, U., Itíe, J.-P. & Spirlet, J. C. (1986). *J. Appl. Cryst.* **19**, 308–310.
Gerward, L., Olsen, J. S., Benedict, U., Luo, H., Itié, J.-P. & Vogt, O. (1988). *High Temp. High Pressure*, **20**, 545–552.
Gerward, L., Olsen, J. S., Benedict, U. & Luo, H. (1990). *J. Less-Common Met.* **161**, L11–L14.
Gerward, L., Olsen, J. S., Steenstrup, S., Benedict, U. & Dabos-Seignon, S. (1990). *J. Appl. Cryst.* **23**, 515–519.
Gupta, D. C. & Singh, K. C. (2010). *Solid State Sci.* **12**, 1809–1815.
Hasegawa, A. & Yamagami, H. (1990). *J. Phys. Soc. Jpn.* **59**, 218–223.
Hedin, L. & Lundqvist, S. (1969). *Solid State Physics*, edited by H. Ehrenreich, F. Seitz & D. Turnbull, Vol. 23, pp. 1–181. New York: Academic Press.
Kanchana, V., Vaitheeswaran, G., Svane, A. & Delin, A. (2006). *J. Phys. Condens. Matter*, **18**, 9615.
Kanchana, V., Vaitheeswaran, G., Zhang, X., Ma, Y., Svane, A. & Eriksson, O. (2011). *Phys. Rev. B*, **84**, 205135.
Kotani, T., van Schilfgaarde, M. & Faleev, S. V. (2007). *Phys. Rev. B*, **76**, 165106.
Kumar, S. & Auluck, S. (2003). *Bull. Mater. Sci.* **26**, 165–168.
Methfessel, M., van Schilfgaarde, M. & Casali, R. A. (2000). *Lecture Notes in Physics*, edited by H. Dreysse, Vol. 535, pp. 114–147. Berlin: Springer-Verlag.
Modak, P. & Verma, A. K. (2011). *Phys. Rev. B*, **84**, 024108.
Nordström, L., Wills, J. M., Andersson, P. H., Söderlind, P. & Eriksson, O. (2000). *Phys. Rev. B*, **63**, 035103.
Olsen, J. S., Steenstrup, S., Gerward, L., Benedict, U. & Itié, J.-P. (1986). *Physica B*, **139–140**, 308–310.
Olsen, J. S., Gerward, L., Benedict, U., Luo, H. & Vogt, O. (1988). *High Temp. High Pressure*, **20**, 553–559.

Olsen, J. S., Gerward, L., Benedict, U., Luo, H. & Vogt, O. (1989). *J. Appl. Cryst.* **22**, 61–63.
Perdew, J. P., Burke, K. & Ernzerhof, M. (1996). *Phys. Rev. Lett.* **77**, 3865–3868.
Petit, L., Svane, A., Szotek, Z., Temmerman, W. M. & Stocks, G. M. (2009). *Phys. Rev. B*, **80**, 045124.
Savrasov, S. Y. (1996). *Phys. Rev. B*, **54**, 16470–16486.
Shein, I. R., Shein, K. I. & Ivanovskii, A. L. (2007). *Tech. Phys. Lett.* **33**, 128–131.
Shein, I. R. & Ivanovskii, A. L. (2010). *Solid State Sci.* **12**, 2106–2112.
Svane, A., Christensen, N. E., Cardona, M., Chantis, A. N., van Schilfgaarde, M. & Kotani, T. (2010). *Phys. Rev. B*, **81**, 245120.
Wedgwood, F. A. (1974). *J. Phys. Solid State Phys.* **7**, 3203–3218.